Published in final edited form as:
Neuron. 2015 February 18; 85(4): 755–769. doi:10.1016/j.neuron.2014.12.057.

The adhesion GPCR GPR126 has distinct, domain-dependent functions in Schwann cell development mediated by interaction with Laminin-211

Sarah C. Petersen[1,*], **Rong Luo**[2,*], **Ines Liebscher**[3,*], **Stefanie Giera**[2], **Sung-jin Jeong**[2,6], **Amit Mogha**[1], **Monica Ghidinelli**[4], **M. Laura Feltri**[4], **Torsten Schöneberg**[3], **Xianhua Piao**[2,**], and **Kelly R. Monk**[1,5,**]

[1]Department of Developmental Biology, Washington University School of Medicine, St. Louis, MO 63110, USA

[2]Division of Newborn Medicine, Department of Medicine, Children's Hospital and Harvard Medical School, Boston, MA 02115, USA

[3]Institute of Biochemistry, Medical Faculty, University of Leipzig, 04103 Leipzig, Germany

[4]Department of Biochemistry, University of Buffalo, The State University of New York, Buffalo, NY 14023, USA

[5]Hope Center for Neurological Disorders, Washington University School of Medicine, St. Louis, MO 63110, USA

SUMMARY

Myelin ensheathes axons to allow rapid propagation of action potentials and proper nervous system function. In the peripheral nervous system, Schwann cells (SCs) radially sort axons into a 1:1 relationship before wrapping an axonal segment to form myelin. SC myelination requires the adhesion G protein-coupled receptor GPR126, which undergoes autoproteolytic cleavage into an N-terminal fragment (NTF) and a 7-transmembrane-containing C-terminal fragment (CTF). Here, we show that GPR126 has domain-specific functions in SC development whereby the NTF is necessary and sufficient for axon sorting while the CTF promotes wrapping through cAMP elevation. These biphasic roles of GPR126 are governed by interactions with Laminin-211, which we define as a novel ligand for GPR126 that modulates receptor signaling via a tethered agonist.

[**]Correspondence should be directed to Xianhua Piao, Xianhua.Piao@childrens.harvard.edu or Kelly R. Monk, monkk@wustl.edu.
[6]Present address: Convergence Brain research Department, Korea Brain Research Institute (KBRI), Daegu, South Korea
[*]Equal contributions

AUTHOR CONTRIBUTIONS

SCP, RL, IL, AM, TS, XP, and KRM designed experiments; SCP, RL, SG, SJ, AM, IL, MG, LMF, and KRM performed experiments; SCP, RL, IL, AM, TS, XP, and KRM analyzed results; SCP, IL, XP, and KRM wrote the paper; all authors edited and approved of the manuscript.

The authors declare no conflicts of interest.

Our work suggests a model in which Laminin-211 mediates GPR126-induced cAMP levels to control early and late stages of SC development.

INTRODUCTION

Myelination in the peripheral nervous system requires radial sorting of axons by Schwann cells (SCs) into a 1:1 relationship followed by spiral wrapping of SC membrane to form the myelin sheath (Jessen and Mirsky, 2005). These processes depend on deposition and maturation of the SC basal lamina (BL) (Bunge et al., 1990; Bunge et al., 1986; Cornbrooks et al., 1983; Feltri and Wrabetz, 2005), which provides mechanical support and a scaffold for signaling pathways that mediate SC development (Carey et al., 1986; Chernousov et al., 2008; Yurchenco, 2011). Underscoring the significance of the BL, disruption of extracellular matrix (ECM) proteins or their interacting partners results in radial sorting and myelination deficits in mouse models (Berti et al., 2011; Court et al., 2006; McKee et al., 2012; Pellegatta et al., 2013), and mutations in genes encoding ECM proteins and their receptors cause congenital muscular dystrophy and dysmyelination in humans (Feltri and Wrabetz, 2005).

SCs synthesize a BL consisting of Laminins (Cornbrooks et al., 1983), Collagen IV (Carey et al., 1983), and heparin sulfate proteoglycans (HSPGs) (Eldridge et al., 1986; Mehta et al., 1985). Initially, the developing BL is discontinuous (Grove and Brophy, 2014). Laminin-211 and axonal signals result in the secretion of Laminin-411, Collagen IV, and HSPGs, as well as additional Laminin-211 that polymerizes to form a dense BL on myelinating SCs (Bunge et al., 1990). Laminin-211 is a heterotrimeric protein composed of α2, β1, and γ1 chains, encoded by *Lama2*, *Lamb1*, and *Lamc1* genes, respectively (Feltri and Wrabetz, 2005). Knockout of *Lama2* or *Lama4* or SC-specific deletion of *Lamc1* all result in radial sorting defects and subsequent myelin impairments (Bradley and Jenkison, 1973; Chen and Strickland, 2003; Wallquist et al., 2005; Yang et al., 2005), as do mutations in genes encoding the Laminin-211 receptors *β1 Integrin* and *α-Dystroglycan* and their effector *Fak* (Berti et al., 2011; Feltri et al., 2002; Grove et al., 2007; Pellegatta et al., 2013).

Adhesion GPCRs (aGPCRs) are a newly defined family of receptors that can mediate cell-ECM interactions. Structurally, aGPCRs are defined by a large extracellular N-terminus and a GPCR autoproteolysis-inducing (GAIN) domain that cleaves the receptor into an N-terminal fragment (NTF) and a 7-transmembrane (7TM)-containing C-terminal fragment (CTF) during the maturation process (Langenhan et al., 2013). Importantly, key amino acids (aa) in the CTF portion of the GAIN domain, termed the *Stachel* sequence (German word for “stinger”), can function as a tethered agonist for CTF activation, and *Stachel*-mediated signaling is essential for SC myelination (Liebscher et al., 2014). The cleaved NTF is non-covalently associated with the CTF at the cell membrane, and crystal structure analyses of aGPCRs demonstrate that the *Stachel* sequence is physically embedded within the N-terminal portion of the GAIN domain (Arac et al., 2012). Additionally, the NTF can partially suppress CTF signaling, and NTF binding partner interactions can modulate CTF signaling (Langenhan et al., 2013; Luo et al., 2014), which may or may not require *Stachel*-mediated activation. Finally, the NTF of aGPCRs can function independently of the CTF

(Promel et al., 2012), and we recently demonstrated bimodal functions of the NTF and CTF of GPR126 in heart development (Patra et al., 2013).

We previously showed that the aGPCR GPR126 is required for SC development and myelination in zebrafish and mouse (Monk et al., 2009; Monk et al., 2011). GPR126 functions in SCs by elevating cAMP via G_s-protein signaling to activate Protein kinase A (PKA) and initiates a terminal differentiation transcription factor cascade including *Oct6* (*Pou3f1*) and *Krox20* (*Egr2*) (Glenn and Talbot, 2013; Mogha et al., 2013). We observed defects in radial sorting and myelination in mouse mutants where both the NTF and CTF are deleted (Monk et al., 2011). However, in zebrafish *gpr126*^{st49} mutants, which are predicted to possess an NTF but not a CTF, SCs fail to myelinate but still sort axons (Monk et al., 2009).

Here we show that GPR126-NTF promotes radial sorting independent of the CTF. By creating a structure-function allelic series of *gpr126* mutants, we demonstrate that the NTF is necessary and sufficient for radial sorting, while the CTF specifically elevates cAMP to drive terminal differentiation. Given that mutations in both *Gpr126* and *Lama2* result in radial sorting defects and because aGPCRs often bind ECM molecules (e.g., Luo et al., 2011), we hypothesized that GPR126 and Laminin-211 may direct these processes via physical interaction and domain-dependent functions of GPR126. We demonstrate that Laminin-211 binds GPR126-NTF and can either suppress or promote *Stachel*-mediated activation of GPR126-CTF. This bimodal role depends upon Laminin-211 concentration and mechanical stimulation *in vitro*, and Laminin-211 polymerization is necessary for myelination via Gpr126 *in vivo*. Together, these data support a model of SC development in which GPR126-NTF directs radial sorting independently of GPR126-CTF, and GPR126-Laminin-211 interactions regulate terminal differentiation and myelination by ensuring appropriate levels of cAMP for a given stage of SC development.

RESULTS

Generation of a zebrafish ΔNTF mutant

The phenotypic differences between mouse and zebrafish mutants with distinct molecular lesions led us to hypothesize that GPR126-NTF has a CTF-independent role in radial sorting. The targeted deletion in *Gpr126*$^{-/-}$ mice produces an early premature stop codon that results in the near-absence of *Gpr126*-NTF mRNA and impaired radial sorting and myelination (Mogha et al., 2013; Monk et al., 2011). In contrast, the zebrafish *gpr126*^{st49} allele is a point mutation that converts a tyrosine to a stop codon near the GPS (Monk et al., 2009) (Figure 1A), such that the NTF is conceivably intact while the CTF signaling domain is absent. Importantly, *gpr126* NTF transcript is detected in homozygous *gpr126*^{st49} zebrafish, and these mutants completely ensheathe a single axon within the field of view (defined as radial sorting in zebrafish, see Supplemental Information) (Monk et al., 2009). Thus, we predicted that differences in radial sorting phenotypes in these *gpr126* zebrafish and mouse mutants could be due to a domain-specific role of the NTF.

To test this, we used TALENs to create a stop codon early in the zebrafish Gpr126-NTF. The *gpr126*^{stl47} allele we generated is a 5+3 insertion-deletion (indel) at Gln68 that produces

a frameshift and truncates the protein in the CUB domain (Figure 1A–C, Figure S1A–B). Morphologically, *gpr126*^{stl47} mutants are grossly normal with some cardiac edema (Figure S1C) and the puffy ear phenotype previously observed in *gpr126*^{st49} mutants (not shown) (Monk et al., 2009). *gpr126*^{stl47} mutants also phenocopy *gpr126*^{st49} with respect to gene expression defects during SC development. Whereas SCs migrate normally in *gpr126*^{stl47} mutants, as marked by expression of *sox10* in the posterior lateral line nerve (PLLn), they fail to express late differentiation markers, such as *krox20* and *mbp* (Figure S1D–J). Furthermore, we noted a more prominent phenotype in maternal-zygotic (MZ) mutants, which are the progeny of a homozygous mutant female. Unlike zygotic (Z) mutants, MZ mutants have no maternal deposition of wild-type (WT) mRNA or protein into the egg. We observed Z mutants have less pronounced defects in *krox20* and *mbp* expression than MZ mutants, suggesting maternal contribution of *gpr126* mRNA or protein partially rescues *gpr126*^{stl47} Z mutants (Figure S1J).

Gpr126-NTF is necessary and sufficient for radial sorting

To test if Gpr126-NTF is necessary for radial sorting, we performed transmission electron microscopy (TEM) of 5 days post-fertilization (dpf) zebrafish. At this stage, SCs have migrated into the periphery, and many have sorted axons and formed several loose wraps of myelin (Figure 1D, I–J). In accordance with published observations (Monk et al., 2009), we observed that *gpr126*^{st49} MZ mutant SCs undergo radial sorting but arrest at the pro-myelinating state (Figure 1E, I–J). In contrast, we observed that radial sorting was severely perturbed in *gpr126*^{stl47} Z and MZ mutants (Figure 1F–G, I). These defects were accompanied by a near complete absence of myelinated fibers in *gpr126*^{stl47} Z mutants and a complete absence in MZ mutants (Figure 1J). To test whether radial sorting defects in *gpr126*^{stl47} mutants are due to loss of functional NTF, we analyzed transheterozygotes containing a single *st49* allele in trans to an *stl47* allele. In these mutants, radial sorting was significantly rescued to the level of *gpr126*^{st49} MZ mutants (Figure 1H, I), indicating the NTF region contained in a single *gpr126*^{st49} allele is sufficient for radial sorting. Because the number of axons per nerve is unchanged from WT in all mutants (Figure 1K), the reduction in sorted and myelinated axons in *gpr126* mutants is likely not due to developmental delays or differences in the region analyzed along the anterior-posterior axis. Thus, these data support the hypothesis that GPR126-NTF drives radial sorting in both zebrafish and mouse.

Gpr126-NTF drives radial sorting independently of cAMP and p-FAK

Our analysis suggested that NTF-dependent radial sorting proceeds independently of CTF signaling. Thus, our model predicts elevation of cAMP would not rescue radial sorting defects in mutants lacking an NTF. To test this hypothesis, we treated *gpr126*^{stl47} larvae with forskolin (FSK), an adenylyl cyclase activator that globally elevates cAMP. Previous studies have demonstrated that FSK application drives myelination in arrested promyelinating *gpr126*^{st49} mutant SCs (Glenn and Talbot, 2013; Monk et al., 2009). FSK treatment, however, was insufficient to rescue radial sorting or myelination *gpr126*^{stl47} mutants (Figure 2A–G). We also noted that ectopic elevation of cAMP induced expression of *mbp* in SCs of *gpr126*^{stl47} larvae (Figure S2A–E). This suggests that activation of a cAMP-dependent myelin gene expression program is independently driven by CTF

signaling. Furthermore, ectopic activation of this program is not dependent on prior SC sorting, though activation of the program is insufficient to drive myelination in the absence of sorting. Thus, we have identified two distinct roles of Gpr126 domains in myelination: an early, NTF-dependent role in immature SCs for radial sorting, and a later, CTF-dependent signaling role to activate a myelin gene expression program in promyelinating SCs.

Given that Gpr126-NTF does not signal through the CTF to drive radial sorting, we tested whether the NTF employs another known pathway for radial sorting. Association between β1-integrin and its ECM ligand Laminin-211 results in phosphorylation of the downstream effector FAK in many cell types, and loss of any of these components results in radial sorting defects. Thus, we tested the possibility that Gpr126-NTF may also function via FAK activation through association with Laminin-211 and β1-integrin. To this end, we performed immunostaining for phosphorylated FAK (p-FAK) in zebrafish PLLn SCs in WT and *gpr126*^{stl47} mutant larvae (Figure 2H). As expected, we saw strong p-FAK expression in WT SC in the PLLn, but we found no difference in p-FAK levels in *gpr126*^{stl47} mutants (Figure 2I), despite the loss of radial sorting (see Figure 1). Thus, we propose that FAK is activated in parallel to Gpr126-NTF signaling, and that Gpr126-NTF employs another, perhaps novel, pathway for radial sorting.

SCs express a putative ligand of GPR126

We next investigated the ligand(s) that could bind GPR126 to modulate its roles in SC development. It was recently demonstrated that the CUB/PTX-containing region of zebrafish Gpr126-NTF binds Collagen IV (Paavola et al., 2014). Importantly, the NTFs of several aGPCRs have multiple binding partners (Langenhan et al., 2013), and we sought to identify further GPR126-NTF ligands *in vivo*. In addition to the CUB and PTX domains, mammalian GPR126-NTF contains two protein cleavage sites: the autoproteolytic GPS and an S2 site (aa 441 in mouse GPR126) where furin-mediated cleavage occurs (Moriguchi et al., 2004) (Figure 3A). Using a newly developed rabbit anti-GPR126 CTF antibody, we indeed detected the cleaved CTF in vivo in P5 sciatic nerve (Figure 3B). We engineered three human IgG Fc-tagged mouse GPR126-NTF constructs: aa 31–807 (full length Gpr126-NTF, Gpr126$^{N31–807}$), aa 31–438 (N-terminal to the S2 site, Gpr126$^{N31–438}$), and aa 446–807 (C-terminal to the S2 site, Gpr126$^{N446–807}$) (Figure 3A). The fusion constructs were transiently transfected into HEK-293T cells to produce recombinant proteins (Figure 3C), which were used to test ligand binding *in situ* on postnatal day (P) 3 sciatic nerves. Under our staining conditions, we did not detect any binding in the P3 nerves with the CUB and PTX containing GPR126$^{N31–438}$ fragment (Figure 3D). In contrast, the C-terminal half of the Gpr126-NTF, present in GPR126$^{N446–807}$ as well as the full length NTF GPR126$^{N31–807}$, was essential for Gpr126-NTF binding at P3 (Figure 3E–F).

The perinuclear pattern of hFc binding indicated that Gpr126-NTF fragments bind a putative SC ligand. To confirm this, we performed co-labeling on P10 nerves to show that GPR126$^{N446–807}$ co-localizes with SC markers S100β (Figure 3G–H) and MBP (Figure S3A) but not with the axonal marker NF200 or fibroblast marker CD34 (Figure S3B–C). These data suggest that Gpr126-NTF specifically binds a SC-derived ligand.

Laminin-211 is a GPR126 ligand

We hypothesized that Laminin-211 is a ligand of GPR126 during SC development and PNS myelination based on the following observations: (1) the putative ligand of GPR126-NTF at P3 is SC-derived (Figure 3G–H, S3A); (2) Laminin-211 is a major SC-derived ECM protein and aGPCRs often bind ECM proteins; (3) *Lama2* and SC-specific *Lamc1* mutants phenocopy the radial sorting defects observed in *Gpr126* mutant mice and *gpr126*^{stl47} mutant zebrafish. To test this hypothesis, we performed *in vitro* co-immunoprecipitation experiments using GPR126-NTF-hFc fusion proteins. To obtain ample Laminin-211, we used primary mouse astrocyte cultures and meningeal fibroblasts as both cells produce abundant amounts of this protein (Figure S3D). We detected Laminin α2 only in the GPR126$^{N446–807}$ immunocomplex but not in the two negative controls, hFc and GPR126$^{N31–438}$ (Figure S3E). To show that this interaction can occur *in vivo*, we incubated Gpr126-NTF-hFc fusion proteins with P4 sciatic nerve lysate. We again detected Laminin α2 co-immunoprecipitating specifically with GPR126$^{N446–807}$ (Figure 3I). Because Laminin-211 is the only α2-containing Laminin expressed in SCs (Feltri and Wrabetz, 2005), we conclude that GPR126$^{N446–807}$ binds Laminin-211. To further confirm that Laminin-211 is a major GPR126 binding partner during SC development, we performed putative ligand binding *in situ* on P10 sciatic nerves from WT and *Lama2*$^{dy3k/dy3k}$ mice, which are targeted null *Lama2* mutants (Miyagoe et al., 1997). In contrast to WT, we failed to detect robust ligand binding in *Lama2*$^{dy3k/dy3k}$ sciatic nerves (Figure 3J–K). Together, our data demonstrate that Laminin-211 binds a novel Laminin-binding domain in GPR126-NTF between aa 446–807.

Laminin-211 concentration affects Gpr126-dependent myelination *in vitro*

Because Laminin-211 deposition increases with BL maturation during radial sorting and myelination, and because Gpr126 physically interacts with Laminin-211, we next tested how SCs respond to differing levels of Laminin-211 *in vitro*. We co-cultured DRG neurons and SCs from WT and *Gpr126*$^{-/-}$ mutants on either low (0.2 μg/mL) or high (5 μg/mL) Laminin-211 to mimic immature or mature BL, respectively (Grove and Brophy, 2014). Ascorbic acid (AA) was added to further encourage BL formation. WT SCs myelinated axons on both concentrations, but to a greater degree on high Laminin-211 (Figure 4A–B, I). In contrast, *Gpr126*$^{-/-}$ SCs failed to myelinate axons on either concentration (Figure 4C–D, I), suggesting that GPR126 is absolutely essential for myelination downstream of BL maturation. We next characterized the myelination potential of SCs on varying Laminin-211 concentrations with addition of FSK to elevate cAMP. With FSK addition, WT SCs exhibited an increase in MBP expression, regardless of Laminin-211 concentration (Figure 4E–F, I). However, the myelination potential of *Gpr126*$^{-/-}$ SCs was limited by Laminin-211 (Figure 4G–H, I), suggesting that both BL maturation and GPR126 activation are essential for myelination. We also speculate that the incomplete rescue of *Gpr126*$^{-/-}$ SC with FSK on either concentration of Laminin-211 may be due to impaired radial sorting in the absence of Gpr126-NTF.

lama2 knockdown enhances *gpr126* mutant defects

Given our *in vitro* results, we next reasoned that knockdown of *lama2* would enhance myelination deficits observed in *gpr126* mutants *in vivo*. To test this, we used the hypomorphic *gpr126*^{st63} allele, which results in reduced but not absent *mbp* expression (Monk et al., 2009; Pogoda et al., 2006). The *st63* lesion is predicted to convert a conserved cysteine to a tyrosine (Figure 1A), which results in reduced Gpr126 trafficking, signaling, and myelination (Liebscher et al., 2014). By using subthreshold doses of an established morpholino (*lama2* MO, (Pollard et al., 2006)), we reasoned that SC development would be perturbed enough to investigate a genetic relationship between *gpr126* and *lama2*, but without off-target effects or developmental delays.

To assess SC terminal development, we used whole mount *in situ* hybridization (WISH) of PLLn *mbp* expression. At 4 dpf, both uninjected and control-injected WT larvae had strong PLLn *mbp* expression. Importantly, *mbp* expression in homozygous WT (*gpr126*$^{+/+}$) was indistinguishable from heterozygotes (*gpr126*$^{+/st63}$) in control larvae (Figure 5A–B, J). Consistent with previous observations, control-injected mutant *gpr126*^{st63} larvae had reduced PLLn *mbp* expression (Figure 5C, J). To slightly diminish *lama2* expression, we injected a low dose of *lama2* MO (2.5 ng) and found that *mbp* expression was largely unaffected in WT *gpr126*$^{+/+}$ larvae (Figure 5D, J). In contrast, *gpr126*$^{+/st63}$ heterozygotes showed a significant reduction of PLLn *mbp* at this dose compared to WT (Figure 5E, J). *gpr126*$^{st63/st63}$ larvae also exhibited reduced *mbp* with a low dose of *lama2* MO (Figure 5F, J). These data, particularly the effect in heterozygous *gpr126*$^{+/st63}$ larvae, strongly suggest a genetic interaction between *lama2* and *gpr126*. Together with our physical binding data (Figure 3I), we predict decreased *mbp* expression in *gpr126*$^{+/st63}$ heterozygotes is due to reducing the Gpr126-NTF/Laminin-211 interaction (via *lama2* MO) and Gpr126 intracellular signaling (via the *gpr126*^{st63} mutation).

To further test whether *lama2* plays a role in zebrafish SC development similar to its role in mammals, we also injected a high dose (5 ng) of *lama2* MO into WT, *gpr126*$^{+/st63}$, and *gpr126*$^{st63/st63}$ animals. PLLn *mbp* expression was reduced across genotypes with 5 ng of *lama2* MO (Figure 5G–J), consistent with hypomyelination observed in *Lama2* mouse mutants (Bradley and Jenkison, 1973; Stirling, 1975). Again, we observed a significant reduction of *mbp* expression with high *lama2* knockdown in heterozygotes compared to WT (Figure 5H, J), though the effect is less pronounced than low knockdown due to the reduction of *mbp* expression in WT. We validated this result with ultrastructural analysis at 3 dpf and found that radial sorting and myelination are reduced both in *gpr126*$^{+/+}$ (Figure 5K–L, O–P) and *gpr126*$^{st63/st63}$ (Figure 5M–N, O–P) with 5 ng of *lama2* MO, without any changes in axon number (Figure 5Q). We also noted a slight reduction in radial sorting in *gpr126*$^{st63/st63}$ mutants relative to WT, which is likely due to decreased trafficking of the mutant receptor and less Gpr126-NTF at the cell surface (Liebscher et al., 2014). In sum, these data are consistent with a model in which Laminin-211 has dual roles *in vivo* in radial sorting and myelination via Gpr126.

Laminin-211 activates GPR126 via under dynamic conditions *in vitro*

Our previous experiments suggest that Laminin-211 activates G_s signaling via GPR126 because myelination, a cAMP-dependent process, occurs in the presence of Laminin-211 and is impaired in its absence. To test if Laminin-211 activates GPR126 signaling, we performed cAMP accumulation assays in heterologous cells transfected with hGPR126 with purified Laminins. Application of increasing concentrations of Laminin-211 caused, to our surprise, a concentration-dependent decrease of cAMP accumulation (Figure S4A). Chimeric G-protein assays indicated that this cAMP suppression was not mediated by G_i-protein signaling (Figure S4B–C), and we conclude that the observed cAMP reduction through Laminin-211 is caused by a general inhibition of basal GPR126 G_s activation.

We have recently shown that GPR126 is activated through a tethered peptide agonist, the *Stachel* sequence, and that *Stachel*-mediated signaling is essential for SC myelination (Liebscher et al., 2014). Based on crystal structures of related aGPCRs (Arac et al., 2012), as well as the negative effect the NTF can exert on CTF signaling (Langenhan et al., 2013), the tethered *Stachel* agonist is predicted to be masked or stabilized by β-sheets of the GAIN domain, preventing a favorable conformation for CTF signaling. Thus, physical removal of the NTF is likely necessary for *Stachel*-mediated signaling. Therefore, we suspected dynamic forces could facilitate Laminin-211 activation of GPR126. Indeed, increasing vibrations during incubation with Laminin-211 led to a synergistic increase in cAMP accumulation (Figure 6A). This effect was not observed under vibration conditions with a full-length GPR126 mutant $F^{815}A$, which specifically inactivates the *Stachel* sequence (Figure S4D), implying that this dynamic effect of Laminin-211 is governed by *Stachel* activation. Synergistic cAMP accumulation under dynamic conditions was also not observed upon addition of other Laminins (Figure S4E), indicating this activating effect is specific to Laminin-211. We obtained even more pronounced cAMP elevation when applying shaking forces: while shaking alone was sufficient to elevate cAMP in GPR126 transfected cells (presumably due to increased force that removed the NTF and exposed the *Stachel* sequence), addition of Laminin-211 facilitates greater activation (Figure 6B). Together, these data support a model in which Laminin-211 regulates GPR126 by promoting a conformation unfavorable to G_s activation in static conditions, but facilitating *Stachel* sequence-mediated activation of the CTF upon dynamic movement.

Laminin α2 promotes myelination through Gpr126 *in vivo*

We next tested the activation of Gpr126 by Laminin-211 *in vivo*. Because high Laminin-211 concentrations drive myelination *in vitro* (Figure 4) (McKee et al., 2012), we hypothesized that increasing *lama2* levels would rescue the myelination defect in *gpr126*^{st63} hypomorphs. To test this, we used an established zebrafish *lama2* overexpression (OE) construct that expresses membrane-tethered EGFP and secreted mCherry-tagged Lama2 from muscle cells and can rescue muscle defects in *lama2* mutants (Sztal et al., 2012). Because the PLLn is directly adjacent to muscle cells and has no perineurial barrier during radial sorting and myelination (see “muscle” in Figure 6D), ectopic muscle-derived Lama2 could act non-cell-autonomously on SCs for the purposes of this experiment.

We therefore injected *gpr126*^{st63} hypomorphs with the *lama2* OE construct and selected morphologically normal larvae with high Lama2-mCherry expression for further analysis (see methods, Figure S5A–B). WISH analysis of *mbp* expression in uninjected and control-injected 3 dpf siblings showed strong PLLn *mbp* expression in WT and weak PLLn *mbp* expression in *gpr126*$^{st63/st63}$ hypomorphs (Figure S5D–E, H). Injection of 20 pg *lama2* OE construct, however, significantly suppressed the *gpr126*^{st63} PLLn *mbp* expression phenotype (Figure S5F, H).

To confirm that increased *mbp* expression corresponds with an increase in myelination, we performed TEM through PLLn cross-sections at 5 dpf. WT siblings showed many myelinated axons in both uninjected and *lama2* OE-injected larvae (Figure 6C–D, J–K). In contrast, control *gpr126*$^{st63/st63}$ hypomorphs showed significantly fewer myelinated axons, likely due to the CTF point mutation that results in reduced activity (Figure 6F, J–K). We also observed slightly reduced radial sorting in *gpr126*$^{st63/st63}$ mutants (Figure 6I), consistent with our model, as the NTF sequence is intact in *gpr126*^{st63}, but trafficking is reduced (Liebscher et al., 2014). Importantly, the percentage of myelinated axons is significantly reduced among sorted axons (Figure S5I), suggesting that the impaired myelination observed in *gpr126*$^{st63/st63}$ mutants is likely not a secondary consequence of reduced sorting. Interestingly, *lama2* OE in *gpr126*$^{st63/st63}$ mutants was sufficient to partially rescue the hypomyelination phenotype (Figure 6G, J), suggesting that ectopic Laminin-211 expression can facilitate additional signaling through the hypomorphic receptor.

To determine if the effect of *lama2* OE functions through Gpr126 signaling or activation of a parallel pathway, we next injected the *lama2* OE construct into *gpr126*^{st49} mutants, which have normal radial sorting via the NTF but lack a functional CTF and thus arrest at the promyelinating state (Figure 1) (Monk et al., 2009). WISH of 3 dpf larvae revealed that *lama2* OE fails to rescue PLLn *mbp* expression in *gpr126*$^{st49/st49}$ mutants (Figure S5H). Therefore, we propose that the rescued myelination observed in *lama2* OE *st63* hypomorphs is due to enhanced signaling through Gpr126-CTF rather than activation of a parallel pathway.

Laminin α2 polymerization is required for Gpr126-mediated myelination

Our *in vitro* findings that suggested Laminin-211 may physically remove GPR126-NTF to promote signaling (Figure 6A, B), and our *in vivo* findings demonstrated that *lama2* OE can drive Gpr126-dependent myelination (Figure 6G, J). Laminin-211 is secreted by SCs and its polymerization is essential for SC development; *Lama2*^{dy2j} mouse mutants have a spontaneous mutation that leads to aberrant splicing and deletion of the Laminin α2 polymerization domain, and these mice have defects in radial sorting and myelination independent of SC proliferation (Colognato and Yurchenco, 1999; Xu et al., 1994; Yang et al., 2005). We therefore speculated that Laminin α2 polymerization could be an activating force on Gpr126, reminiscent of physical forces in our *in vitro* system. To test this model, we precisely deleted 165 bp from the *lama2* OE construct to mimic the polymerization-defective splice isoform found in *Lama2*^{dy2j} mutants. When the *lama2(dy2j)* OE construct was injected into zebrafish, the resulting mCherry-tagged protein was expressed and

secreted at levels comparable to *lama2* OE (Figure S5B–C). However, unlike WT *lama2*, this polymerization-defective *lama2(dy2j)* allele was not sufficient to rescue myelination defects in *gpr126*$^{st63/st63}$ mutants (Figure 6H, J–K, Figure S5I). Interestingly, *lama2(dy2j)* OE was sufficient to promote *mbp* gene expression at 4 dpf even in the absence of myelination (Figure S5G–H), highlighting potential alternative mechanisms of Gpr126 signaling and activation (e.g., conformational change without NTF removal), as well as further parsing the differences between the myelin gene expression program and physical myelination.

Therefore, we conclude that Laminin α2 polymerization is necessary for Gpr126 activation to drive myelination *in vivo*. Based on our *in vitro* assays, we suggest that polymerization may physically remove the NTF to promote *Stachel*-mediated Gpr126 signaling. Furthermore, our genetic analyses (summarized in Figure S6) support our model that Laminin-211 interacts with Gpr126 to promote myelination.

Taken together, we have shown that Laminin-211 and Gpr126 are required at multiple stages of SC development, and that Laminin-211 can exert both an inhibitory or activating effect on Gpr126-CTF through physical interaction with Gpr126-NTF. We propose that these differential effects of Laminin-211 on GPR126 reflect a model of SC development. Prior to BL maturation, SCs secrete Laminin-211, which interacts with GPR126-NTF to prevent *Stachel* sequence binding and G_s signaling from the CTF. Suppression of G_s signaling could serve to promote an immature and proliferative SC state until radial sorting is complete (Figure 7). Following radial sorting, additional Laminin-211 is deposited and polymerizes, which potentially results in dissociation of the NTF from the CTF and allows the *Stachel* sequence to bind the 7TM domain of the CTF. This promotes G_s-mediated signaling, accumulation of cAMP, and downstream signaling to drive SC terminal differentiation (Figure 7).

DISCUSSION

The essential role of the BL in SC development has been long established. Classic *in vitro* studies show that SCs depend on axon signals to form the BL, and that BL formation is essential for radial sorting and myelination (Bunge, 1983). SCs fail to myelinate axons when co-cultured in serum-free media (Moya et al., 1980), but myelination can be rescued by addition of purified BL to the cultures. Interestingly, when BL components were separated into constituent parts, only Laminin, and not Collagen IV or HSPGs, was sufficient to promote myelination (Eldridge et al., 1989). Subsequent genetic studies have underscored the importance of Laminin in SC biology (Berti et al., 2011; Feltri et al., 2002; Grove et al., 2007; Yurchenco, 2011); however, it has been unclear how SCs exit a premyelinating state to begin wrapping the axon, and how ECM molecules might facilitate this switch. Our work suggests that the aGPCR GPR126 serves as a crucial link between the extracellular environment of SCs and intracellular cAMP accumulation to control SC development.

We have demonstrated that Gpr126-NTF is necessary and sufficient for radial sorting independent of the CTF (Figures 1–2, S2, S6) and that Laminin-211 physically, genetically, and functionally interacts with GPR126 to direct SC development. The physical interaction

of GPR126 with SC-derived Laminin-211 occurs at a previously uncharacterized Laminin α2-binding domain in the glycosylated stalk region of the NTF (Figures 3, S3). We have also shown via multiple assays that Laminin-211 modulates SC differentiation via GPR126 signaling. First, our co-culture studies show that high levels of Laminin-211 facilitate GPR126 signaling to drive myelination (Figure 4). Our cell signaling assays show that Laminin-211 can either suppress or activate cAMP accumulation via GPR126 depending on dynamic movement, suggesting that Laminin-211 interacts with the NTF to facilitate availability of the *Stachel* sequence (Figures 6, S4). Finally, our genetic interaction analyses demonstrate that *lama2* loss- and gain-of-function influence Gpr126-dependent SC terminal differentiation *in vivo*, and importantly, that this interaction is likely mediated by Laminin-211 polymerization and signaling through the CTF (Figures 5–6, S5–S6). Together, our data support a model in which Laminin-211 interacts with GPR126 to mediate its distinct, domain-dependent functions in SC radial sorting and myelination (Figure 7).

While both Laminin-211 and GPR126-NTF are essential for radial sorting (Bradley and Jenkison, 1973; Monk et al., 2011; Mogha et al., 2013; present study), our studies do not formally address whether they fulfill this role by physical interaction in a heteromeric complex. Given the known interactions of Laminin-211 with β1 Integrin (Feltri et al., 2002), one hypothesis could be that GPR126-NTF is a newly identified component within the same extracellular complex that activates FAK to drive radial sorting. Intriguingly, it appears that FAK activation is unchanged in *gpr126* zebrafish mutants, suggesting that GPR126-NTF drives radial sorting independently of FAK. However, it remains possible that GPR126-NTF interacts with β1-integrin but activates a FAK-independent pathway, or perhaps functions in a coordinated function with NRG1-ErbB2/3 signaling. Because cAMP accumulation functions synergistically with ErbB2/3 activation in myelination (Monje et al., 2006), it is possible that Laminin-211 interacts with this pathway, potentially in concert with GPR126-NTF, as well.

Although Laminin-211 is a binding partner of GPR126-NTF in SCs, it likely does not function as an agonist in the classic sense of receptor-ligand interactions. In the case of radial sorting, Laminin-211 may stabilize the non-covalent interaction of the NTF to the CTF, specifically preventing cAMP accumulation in immature SCs by masking the *Stachel* sequence and preventing CTF activation (Figure 7). Together, reported aGPCR crystal structures (Arac et al., 2012), the activation of GPR126 with Laminin-211 under dynamic conditions in our signaling assays, and the requirement of Laminin-211 polymerization in our *in vivo* rescue studies predict a mechanical removal or modulation of GPR126-NTF to activate signaling and cAMP accumulation in SCs. This prediction is consistent with a recent report on the regulation of the aGPCR CD97 by shear stress (Karpus et al., 2013) as well as our recent finding that the GPR56 ligand, collagen III, activates RhoA by removing GPR56-NTF from the cell surface (Luo et al., 2014). NTF removal is favorable for *Stachel* sequence binding to the 7TM, which would result in enhanced G_s signaling and cAMP accumulation, ultimately leading to terminal differentiation and myelination. We suggest that one potential mechanical force driving NTF removal *in vivo* may be increasing Laminin-211 extracellular concentration and subsequent polymerization during BL maturation, which both appear to facilitate Gpr126-regulated myelination in our assays.

Based on aGPCR crystal structures and the strongly hydrophobic residues in the *Stachel* sequence, NTF/CTF dissociation is likely irreversible and would potentially result in a CTF conformation favorable for massive cAMP elevation followed by receptor internalization. We note, however, that *Stachel*-mediated activation is one of several activation modes for GPR126. Perhaps smaller conformational changes, in which the NTF remains associated with the CTF, are also sufficient to activate G_s signaling to a lesser degree (Langenhan et al., 2013). These multiple tiers of Gpr126 activation may underlie our finding that *mbp* expression could be present in the absence of physical myelination (*e.g.* Figure S5G). Additionally, a recent study demonstrated that Collagen IV binds zebrafish Gpr126 and activates signaling in stationary conditions (Paavola et al., 2014), in contrast to our finding that Laminin-211 inhibits signaling in comparable conditions. Interestingly, we found that collagen-mediated cAMP accumulation is apparently minor relative to *Stachel*-mediated signaling (Figure S7). This perhaps highlights the multiple activation mechanisms of GPR126 based on binding partner interactions and suggests that BL constituents may fine-tune cAMP levels via GPR126 throughout SC development.

Our study establishes Laminin-211 as an interacting partner for GPR126 that can prevent or promote *Stachel*-mediated cAMP accumulation. However, other SC-derived ligands, in addition to Collagen IV, may also physically interact with GPR126. With the methodology we applied in this study, we only detected GPR126-NTF binding on SCs. Nevertheless, given that axon signals are required for BL formation and myelination *in vitro* (Bunge et al., 1990; Bunge et al., 1982; Bunge et al., 1980), neuronal GPR126 ligand(s) may exist, as could activating protein(s) presented by neighboring fibroblasts. Future studies, perhaps using different time points and approaches, are required to investigate these possibilities. Moreover, the NTF may also have additional functions, particularly in other GPR126-expressing tissues such as the heart (Patra et al., 2013; Waller-Evans et al., 2010). Although Collagen IV is produced by SCs and binds the CUB-PTX region of Gpr126, our assays did not detect binding CUB-PTX-containing Fc-tagged fragments in SCs at the time-points we examined (Figure 3). Thus, the ligands and activation of GPR126 may differ depending on tissue and developmental stage.

The unique, domain-dependent roles of GPR126 in several stages of SC development solidify this aGPCR as a key regulator of SC development and myelination and point to the bi-functional potential of other aGPCRs. In our study, we have physically, genetically, and functionally connected GPR126 with Laminin-211, another fundamental regulator of SC biology, to show that together they regulate radial sorting and myelination. Mutations in *LAMA2* result in congenital muscular dystrophy in humans, which can be accompanied by dysmyelinating neuropathy. Given the pharmacological power of GPCRs as drug targets, identification of GPR126 ligands (both endogenous and exogenous) and its activating mechanisms could serve as a foundation for developing therapeutics that target SCs in peripheral myelinopathies.

EXPERIMENTAL PROCEDURES

Zebrafish mutant strains and analysis

gpr126^{st49} and *gpr126*^{st63} mutants were described previously (Monk et al., 2009; Pogoda et al., 2006). The *stl47* mutant was generated with the TALEN targeter tool (https://talent.cac.cornell.edu/) and GoldyTALEN kit (Bedell et al., 2012). TALEN mRNA was microinjected at the 1-cell stage and germline-transmitted lesions, including *stl47*, were identified via Sanger sequencing. WISH, immunostaining, and TEM were performed according to standard protocols. All assays were quantified with observer blind to genotype and treatment. Sample numbers and additional methods are provided in the supplement.

GPR126-NTF-Fc constructs

GPR126-NTF-Fc fragments were generated by PCR and fused to hFc. GPR126-NTF-Fc fragments were purified from transfected HEK-293T cells as described (Luo et al., 2011). Equal amounts of hFc-tagged fusion proteins were applied to fresh frozen nerves, putative ligand binding was visualized by fluorescein-conjugated rabbit anti-human IgG antibody (Thermo Scientific). Co-IP and immunoblotting were performed as described (Luo et al., 2011). For IP with nerve homogenate, P3 sciatic nerves were lysed in RIPA buffer. 250 μg of lysate was incubated for 3 hours with hFc or Gpr126-NTF-hFc fusion proteins, followed by 1h with protein G sepharose beads (GE Healthcare). Additional cloning, culture, and purification details are provided in the supplement.

Mouse mutant strains and analysis

Lama2^{dy3k} and *Gpr126* mutants were described previously (Miyagoe et al. 1997; Monk et al. 2011). E12.5 DRGs were isolated as described (Mogha et al., 2013) and cultured on indicated concentrations of Laminin-211 (following Grove and Brophy, 2014). Immunohistochemistry was performed as described (Jeong et al., 2012). Specific strains, antibodies and genotypes are provided in the supplement.

lama2 modulation in zebrafish

Knockdown of *lama2* and OE of *lama2* and *lama2(dy2j)* were performed in embryos collected from *gpr126*$^{st63/+}$ in-crosses. An established *lama2* translation-blocking morpholino (Pollard et al., 2006) from GeneTools was microinjected at 2.5 and 5 ng to reduce Laminin α2 levels. OE of *lama2* and *lama2(dy2j)* was performed with 10–20 pg of an established *acta1:lama2-mCherry:T2:EGFP-CAAX* construct (Sztal et al., 2012) co-injected with 25–50 pg of Tol2 transposase mRNA (Asakawa et al., 2008). Cloning and scoring details are provided in the supplement.

In vitro functional assays

Human GPR126 was cloned into pcDps expression vector as described (Mogha et al., 2013). Constructs were expressed in COS-7 cells under standard conditions (Liebscher et al., 2014). cAMP assays were performed as described (Mogha et al., 2013). Vibration was applied to cultures with a Heidolph Titramax; shaking was applied in a lab incubator (Edmund Bühler

GmbH; Sh30; TH30). Laminins were purchased from Biolamina or kindly provided by Peter Yurchenco. Specific culture and assay conditions are described in the supplement.

Supplementary Material

Refer to Web version on PubMed Central for supplementary material.

ACKNOWLEDGEMENTS

We thank Monk laboratory members, Eugene Johnson Jr., Steve Johnson, Kevin Monk, Lila Solnica-Krezel, and Andrew Yoo for valuable discussions and feedback. We thank Jimann Shin and Jiakun Chen for assistance with TALEN design, Peter Currie for the *lama2* OE construct, Peter Yurchenco for Laminin-211, Marilyn Levy and Robyn Roth for TEM assistance, and Charleen Johnson, Zack Spence, and the Washington University Zebrafish Consortium staff for excellent zebrafish care. This work was supported by grants from NIH F32 NS087786 (SCP), Leonard and Isabelle Goldenson Research Fellowship Fund (RL), William Randolph Hearst Fund (SJ and RL), University of Leipzig Formel 1 start-up grant (IL), BMBF IFB AdipositasDiseases Leipzig (IL), NIH R01 NS045630 (MLF), Deutsche Forschungsgemeinschaft (FOR 2149, IL, TS), Cerebral Palsy International Research Foundation (XP), Muscular Dystrophy Association 293295 (XP and KRM), and NIH R01 NS079445 (KRM).

REFERENCES

Arac D, Boucard AA, Bolliger MF, Nguyen J, Soltis SM, Sudhof TC, Brunger AT. A novel evolutionarily conserved domain of cell-adhesion GPCRs mediates autoproteolysis. EMBO J. 2012; 31:1364–1378. [PubMed: 22333914]

Asakawa K, Suster ML, Mizusawa K, Nagayoshi S, Kotani T, Urasaki A, Kishimoto Y, Hibi M, Kawakami K. Genetic dissection of neural circuits by Tol2 transposon-mediated Gal4 gene and enhancer trapping in zebrafish. Proc Natl Acad Sci U S A. 2008; 105:1255–1260. [PubMed: 18202183]

Bedell VM, Wang Y, Campbell JM, Poshusta TL, Starker CG, Krug Ii RG, Tan W, Penheiter SG, Ma AC, Leung AY, et al. In vivo genome editing using a high-efficiency TALEN system. Nature. 2012

Berti C, Bartesaghi L, Ghidinelli M, Zambroni D, Figlia G, Chen ZL, Quattrini A, Wrabetz L, Feltri ML. Non-redundant function of dystroglycan and beta1 integrins in radial sorting of axons. Development. 2011; 138:4025–4037. [PubMed: 21862561]

Bradley WG, Jenkison M. Abnormalities of peripheral nerves in murine muscular dystrophy. J Neurol Sci. 1973; 18:227–247. [PubMed: 4120487]

Bunge MB, Clark MB, Dean AC, Eldridge CF, Bunge RP. Schwann cell function depends upon axonal signals and basal lamina components. Ann N Y Acad Sci. 1990; 580:281–287. [PubMed: 2337301]

Bunge MB, Williams AK, Wood PM. Neuron-Schwann cell interaction in basal lamina formation. Developmental biology. 1982; 92:449–460. [PubMed: 7117693]

Bunge MB, Williams AK, Wood PM, Uitto J, Jeffrey JJ. Comparison of nerve cell and nerve cell plus Schwann cell cultures, with particular emphasis on basal lamina and collagen formation. J Cell Biol. 1980; 84:184–202. [PubMed: 7188611]

Bunge RP. Recent observations on the control of Schwann cell functions. Anat Rec Suppl. 1983; 1:3–25. [PubMed: 6586088]

Bunge RP, Bunge MB, Eldridge CF. Linkage between axonal ensheathment and basal lamina production by Schwann cells. Annu Rev Neurosci. 1986; 9:305–328. [PubMed: 3518587]

Carey DJ, Eldridge CF, Cornbrooks CJ, Timpl R, Bunge RP. Biosynthesis of type IV collagen by cultured rat Schwann cells. J Cell Biol. 1983; 97:473–479. [PubMed: 6885907]

Carey DJ, Todd MS, Rafferty CM. Schwann cell myelination: induction by exogenous basement membrane-like extracellular matrix. J Cell Biol. 1986; 102:2254–2263. [PubMed: 3086325]

Chen ZL, Strickland S. Laminin gamma1 is critical for Schwann cell differentiation, axon myelination, and regeneration in the peripheral nerve. J Cell Biol. 2003; 163:889–899. [PubMed: 14638863]

Chernousov MA, Yu WM, Chen ZL, Carey DJ, Strickland S. Regulation of Schwann cell function by the extracellular matrix. Glia. 2008; 56:1498–1507. [PubMed: 18803319]

Colognato H, Yurchenco PD. The laminin alpha2 expressed by dystrophic dy(2J) mice is defective in its ability to form polymers. Current biology : CB. 1999; 9:1327–1330. [PubMed: 10574769]

Cornbrooks CJ, Carey DJ, McDonald JA, Timpl R, Bunge RP. In vivo and in vitro observations on laminin production by Schwann cells. Proc Natl Acad Sci U S A. 1983; 80:3850–3854. [PubMed: 6344090]

Court FA, Wrabetz L, Feltri ML. Basal lamina: Schwann cells wrap to the rhythm of space-time. Current opinion in neurobiology. 2006; 16:501–507. [PubMed: 16956757]

Eldridge CF, Bunge MB, Bunge RP. Differentiation of axon-related Schwann cells in vitro: II. Control of myelin formation by basal lamina. J Neurosci. 1989; 9:625–638. [PubMed: 2918381]

Eldridge CF, Sanes JR, Chiu AY, Bunge RP, Cornbrooks CJ. Basal lamina-associated heparan sulphate proteoglycan in the rat PNS: characterization and localization using monoclonal antibodies. J Neurocytol. 1986; 15:37–51. [PubMed: 2940343]

Feltri ML, Graus Porta D, Previtali SC, Nodari A, Migliavacca B, Cassetti A, Littlewood-Evans A, Reichardt LF, Messing A, Quattrini A, et al. Conditional disruption of beta 1 integrin in Schwann cells impedes interactions with axons. J Cell Biol. 2002; 156:199–209. [PubMed: 11777940]

Feltri ML, Wrabetz L. Laminins and their receptors in Schwann cells and hereditary neuropathies. J Peripher Nerv Syst. 2005; 10:128–143. [PubMed: 15958125]

Glenn TD, Talbot WS. Analysis of Gpr126 function defines distinct mechanisms controlling the initiation and maturation of myelin. Development. 2013; 140:3167–3175. [PubMed: 23804499]

Grove M, Brophy PJ. FAK Is Required for Schwann Cell Spreading on Immature Basal Lamina to Coordinate the Radial Sorting of Peripheral Axons with Myelination. J Neurosci. 2014; 34:13422–13434. [PubMed: 25274820]

Grove M, Komiyama NH, Nave KA, Grant SG, Sherman DL, Brophy PJ. FAK is required for axonal sorting by Schwann cells. J Cell Biol. 2007; 176:277–282. [PubMed: 17242067]

Jeong SJ, Luo R, Li S, Strokes N, Piao X. Characterization of G protein-coupled receptor 56 protein expression in the mouse developing neocortex. J Comp Neurol. 2012; 520:2930–2940. [PubMed: 22351047]

Jessen KR, Mirsky R. The origin and development of glial cells in peripheral nerves. Nat Rev Neurosci. 2005; 6:671–682. [PubMed: 16136171]

Karpus ON, Veninga H, Hoek RM, Flierman D, van Buul JD, Vandenakker CC, vanBavel E, Medof ME, van Lier RA, Reedquist KA, et al. Shear stress-dependent downregulation of the adhesion-G protein-coupled receptor CD97 on circulating leukocytes upon contact with its ligand CD55. J Immunol. 2013; 190:3740–3748. [PubMed: 23447688]

Langenhan T, Aust G, Hamann J. Sticky signaling--adhesion class G protein-coupled receptors take the stage. Sci Signal. 2013; 6:re3. [PubMed: 23695165]

Liebscher I, Schön J, Petersen SC, Fischer L, Auerbach N, Demberg LM, Mogha A, Cöster M, Simon K-U, Rothemund S, et al. A tethered agonist within the ectodomain activates the adhesion G protein-coupled receptors GPR126 and GPR133. Cell Rep. 2014 in press.

Luo R, Jeong SJ, Jin Z, Strokes N, Li S, Piao X. G protein-coupled receptor 56 and collagen III, a receptor-ligand pair, regulates cortical development and lamination. Proc Natl Acad Sci U S A. 2011; 108:12925–12930. [PubMed: 21768377]

Luo R, Jeong SJ, Yang A, Wen M, Saslowsky DE, Lencer WI, Arac D, Piao X. Mechanism for adhesion G protein-coupled receptor GPR56-mediated RhoA activation induced by collagen III stimulation. PLoS One. 2014; 9:e100043. [PubMed: 24949629]

McKee KK, Yang DH, Patel R, Chen ZL, Strickland S, Takagi J, Sekiguchi K, Yurchenco PD. Schwann cell myelination requires integration of laminin activities. J Cell Sci. 2012; 125:4609–4619. [PubMed: 22767514]

Mehta H, Orphe C, Todd MS, Cornbrooks CJ, Carey DJ. Synthesis by Schwann cells of basal lamina and membrane-associated heparan sulfate proteoglycans. J Cell Biol. 1985; 101:660–666. [PubMed: 3160714]

Miyagoe Y, Hanaoka K, Nonaka I, Hayasaka M, Nabeshima Y, Arahata K, Takeda S. Laminin alpha2 chain-null mutant mice by targeted disruption of the Lama2 gene: a new model of merosin (laminin 2)-deficient congenital muscular dystrophy. FEBS Lett. 1997; 415:33–39. [PubMed: 9326364]

Mogha A, Benesh AE, Patra C, Engel FB, Schoneberg T, Liebscher I, Monk KR. Gpr126 functions in Schwann cells to control differentiation and myelination via G-protein activation. J Neurosci. 2013; 33:17976–17985. [PubMed: 24227709]

Monje PV, Bartlett Bunge M, Wood PM. Cyclic AMP synergistically enhances neuregulin-dependent ERK and Akt activation and cell cycle progression in Schwann cells. Glia. 2006; 53:649–659. [PubMed: 16470843]

Monk KR, Naylor SG, Glenn TD, Mercurio S, Perlin JR, Dominguez C, Moens CB, Talbot WS. A G protein-coupled receptor is essential for Schwann cells to initiate myelination. Science. 2009; 325:1402–1405. [PubMed: 19745155]

Monk KR, Oshima K, Jors S, Heller S, Talbot WS. Gpr126 is essential for peripheral nerve development and myelination in mammals. Development. 2011; 138:2673–2680. [PubMed: 21613327]

Moriguchi T, Haraguchi K, Ueda N, Okada M, Furuya T, Akiyama T. DREG, a developmentally regulated G protein-coupled receptor containing two conserved proteolytic cleavage sites. Genes Cells. 2004; 9:549–560. [PubMed: 15189448]

Moya F, Bunge MB, Bunge RP. Schwann cells proliferate but fail to differentiate in defined medium. Proc Natl Acad Sci U S A. 1980; 77:6902–6906. [PubMed: 6935691]

Paavola KJ, Sidik H, Zuchero JB, Eckart M, Talbot WS. Type IV collagen is an activating ligand for the adhesion G protein-coupled receptor GPR126. Sci Signal. 2014; 7:ra76. [PubMed: 25118328]

Patra C, van Amerongen MJ, Ghosh S, Ricciardi F, Sajjad A, Novoyatleva T, Mogha A, Monk KR, Muhlfeld C, Engel FB. Organ-specific function of adhesion G protein-coupled receptor GPR126 is domain-dependent. Proc Natl Acad Sci U S A. 2013; 110:16898–16903. [PubMed: 24082093]

Pellegatta M, De Arcangelis A, D'Urso A, Nodari A, Zambroni D, Ghidinelli M, Matafora V, Williamson C, Georges-Labouesse E, Kreidberg J, et al. alpha6beta1 and alpha7beta1 integrins are required in Schwann cells to sort axons. J Neurosci. 2013; 33:17995–18007. [PubMed: 24227711]

Pogoda HM, Sternheim N, Lyons DA, Diamond B, Hawkins TA, Woods IG, Bhatt DH, Franzini-Armstrong C, Dominguez C, Arana N, et al. A genetic screen identifies genes essential for development of myelinated axons in zebrafish. Dev Biol. 2006; 298:118–131. [PubMed: 16875686]

Pollard SM, Parsons MJ, Kamei M, Kettleborough RN, Thomas KA, Pham VN, Bae MK, Scott A, Weinstein BM, Stemple DL. Essential and overlapping roles for laminin alpha chains in notochord and blood vessel formation. Developmental biology. 2006; 289:64–76. [PubMed: 16321372]

Promel S, Frickenhaus M, Hughes S, Mestek L, Staunton D, Woollard A, Vakonakis I, Schoneberg T, Schnabel R, Russ AP, et al. The GPS Motif Is a Molecular Switch for Bimodal Activities of Adhesion Class G Protein-Coupled Receptors. Cell Rep. 2012; 2:321–331. [PubMed: 22938866]

Stirling CA. Abnormalities in Schwann cell sheaths in spinal nerve roots of dystrophic mice. J Anat. 1975; 119:169–180. [PubMed: 1133086]

Sztal TE, Sonntag C, Hall TE, Currie PD. Epistatic dissection of laminin-receptor interactions in dystrophic zebrafish muscle. Hum Mol Genet. 2012; 21:4718–4731. [PubMed: 22859503]

Waller-Evans H, Promel S, Langenhan T, Dixon J, Zahn D, Colledge WH, Doran J, Carlton MB, Davies B, Aparicio SA, et al. The orphan adhesion-GPCR GPR126 is required for embryonic development in the mouse. PLoS One. 2010; 5:e14047. [PubMed: 21124978]

Wallquist W, Plantman S, Thams S, Thyboll J, Kortesmaa J, Lannergren J, Domogatskaya A, Ogren SO, Risling M, Hammarberg H, et al. Impeded interaction between Schwann cells and axons in the absence of laminin alpha4. J Neurosci. 2005; 25:3692–3700. [PubMed: 15814800]

Xu H, Wu XR, Wewer UM, Engvall E. Murine muscular dystrophy caused by a mutation in the laminin alpha 2 (Lama2) gene. Nat Genet. 1994; 8:297–302. [PubMed: 7874173]

Yang D, Bierman J, Tarumi YS, Zhong YP, Rangwala R, Proctor TM, Miyagoe-Suzuki Y, Takeda S, Miner JH, Sherman LS, et al. Coordinate control of axon defasciculation and myelination by laminin-2 and -8. J Cell Biol. 2005; 168:655–666. [PubMed: 15699217]

Yurchenco PD. Basement membranes: cell scaffoldings and signaling platforms. Cold Spring Harb Perspect Biol. 2011; 3

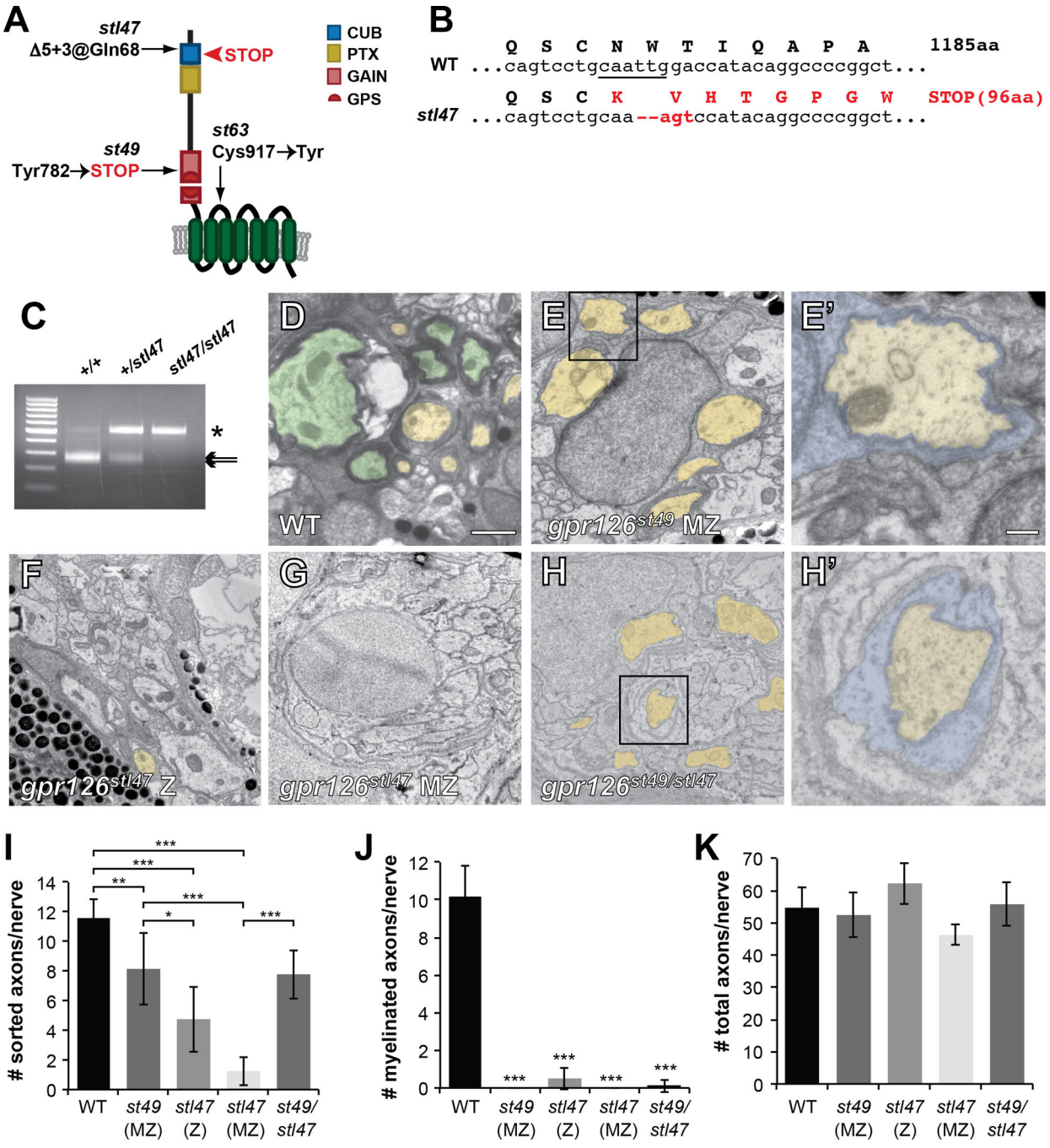

Figure 1. Gpr126-NTF is necessary and sufficient for radial sorting

(**A**) Schematic representation of zebrafish Gpr126 showing *stl47*, *st49*, and *st63* alleles. Red arrowhead shows STOP codon in *stl47*. (**B**) Sequence of WT vs. *gpr126*^{stl47} alleles. WT *gpr126* encodes an 1185 aa protein. *stl47* has a Δ5+3 indel that truncates the protein at aa 96. The TALEN-targeted MfeI site is underlined. (**C**) Restriction fragment length analysis to genotype *gpr126*^{stl47}. WT PCR product is cleaved into 257 and 241 bp fragments by MfeI (arrows). *stl47* retains the undigested 498 bp product (asterisk). (**D–H**) TEM of 5 dpf zebrafish showing cross-sections through PLLn. Boxed regions in E, H indicate

magnification in E', H'. Scale bar = 1 μm except E', H' scale bar = 0.2 μm. (**D**) Axons are sorted (pseudocolored yellow) and myelinated (pseudocolored green) in a WT nerve. (**E**) SCs (blue in E') sort axons but arrest at the promyelinating state in a maternal-zygotic (MZ) *gpr126*^{st49} mutant. (**F**) Both radial sorting and myelination are impaired in zygotic (Z) and (**G**) MZ *gpr126*^{stl47} mutants. (**H**) Radial sorting is rescued in a *gpr126*$^{stl49/stl47}$ transheterozygote. (**I–K**) Quantification of TEM images. Bars represent means ± SD. * $p<0.05$, ** $p<0.01$, *** $p<0.001$, 1-way ANOVA with Bonferroni's multiple comparisons test. (**I**) Number of sorted axons (ensheathed by 1–1.5 wraps SC cytoplasm) per PLLn. (**J**) Number of myelinated axons (>1.5 wraps SC cytoplasm) per PLLn. All mutants were compared to WT for statistical analysis. (**K**) Number of total axons per PLLn.

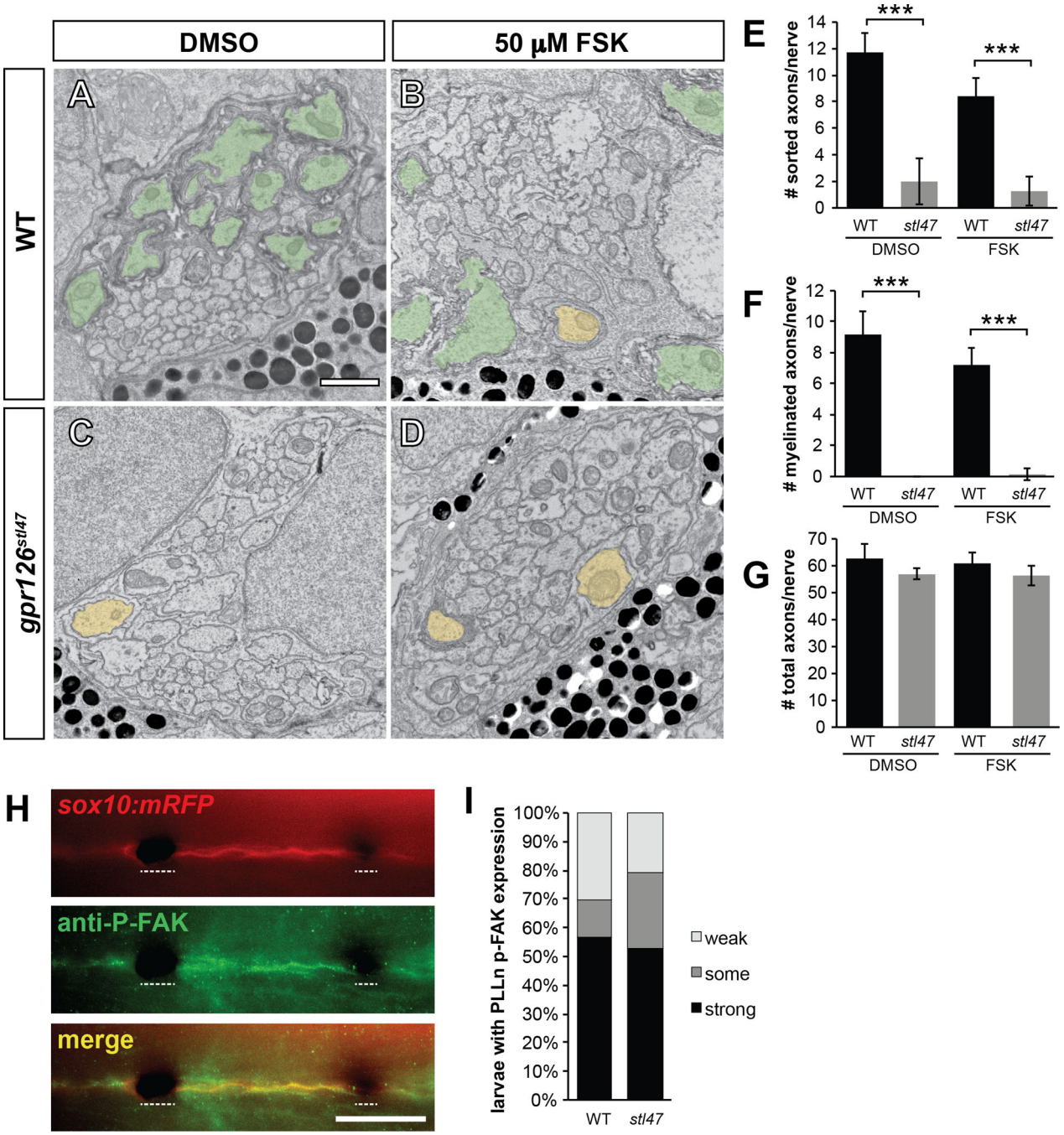

Figure 2. Gpr126-NTF radial sorting occurs independently of Gpr126-CTF and p-FAK signalling

(**A–D**) TEM of 5 dpf zebrafish showing cross-sections through PLLn. Sorted and myelinated axons are defined and pseudocolored as in Figure 1. Scale bar = 1 µm. (**A**) Radial sorting and myelination are observed in WT siblings treated with DMSO and (**B**) 50 µM forskolin (FSK). (**C**) Radial sorting and myelination are impaired in *gpr126*^{stl47} zygotic mutant siblings treated with DMSO and (**D**) FSK. (**E–G**) Quantification of TEM images. Bars represent means ± SD. *** p<0.001, 1-way ANOVA with Bonferroni's multiple

comparisons test. (**E**) Number of sorted axons per PLLn. (**F**) Number of myelinated axons per PLLn. (**G**) Number of total axons per PLLn. (**H**) Phosphorylated FAK (P-FAK) immunostaining (green) labels PLLn SCs of a 4 dpf WT *Tg(sox10:mRFP)* larva (red). Dotted lines indicate regions where pigment cells obscure fluorescence. Scale bar = 100 μm. (**I**) Quantification of p-FAK levels expressed as a percentage of larvae with SC-specific p-FAK immunostaining along the PLLn in WT and *gpr126*^{stl47} mutants. No significant difference was observed in either genotype.

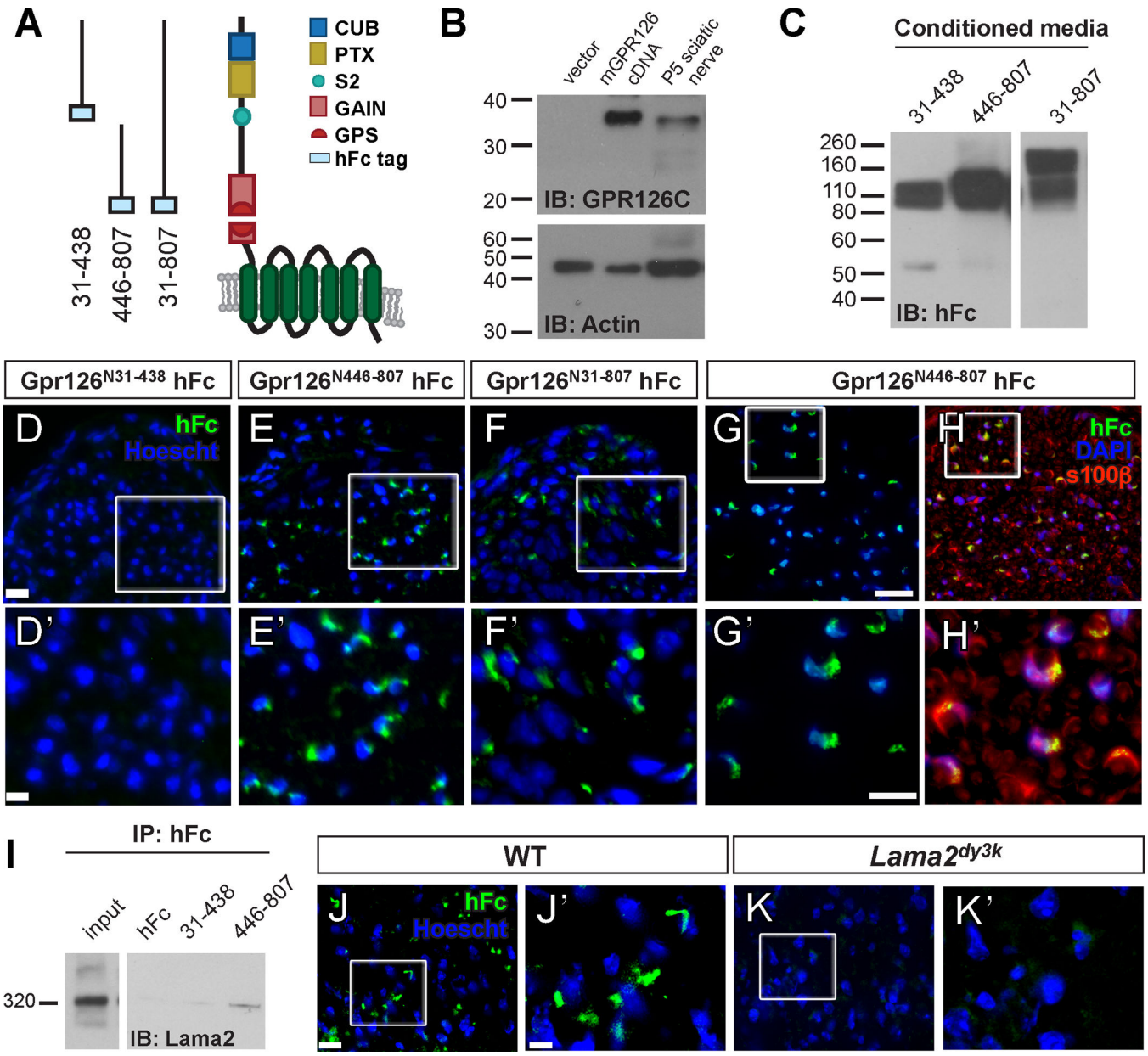

Figure 3. GPR126-NTF binds SC-derived Lama2

(**A**) Diagram showing domains in human GPR126-NTF and fusion constructs for three different GPR126-NTF fragments. (**B**) Detection of GPR126 cleavage *in vitro* and *in vivo*. P6 mouse sciatic nerve and 293T cells transfected with either mouse *Gpr126* cDNA or empty vector were lysed and immunoblotted with rabbit anti-GPR126 CTF antibody. A specific 35 kDa GPR126 CTF was detected in *Gpr126* transfected cells and in P6 mouse sciatic nerve. (**C**) Fusion constructs were transfected into HEK-293T cells to generate fusion recombinant proteins. Purified proteins were verified by western blot. Two bands were detected in GPR126$^{N31–807}$ transfected media due to the second cleavage between aa 440 and 441; the higher band is full length NTF. (**D–F**) Putative ligand binding on P3 sciatic nerves. Anti-hFc immunostaining is green and nuclear counterstain is Hoechst 33342 (blue).

Magnification of boxed regions in **D–F** (scale bar = 20 μm) is indicated in **D'–F'** (scale bar = 10 μm). (**D**) No binding was detected with the GPR126$^{N31–438}$ hFc fragment. (**E**) The GPR126$^{N446–807}$ and (**F**) full-length GPR126$^{N31–807}$ hFc fragments reveal the same ligand binding pattern. (**G–H**) The GPR126$^{N446–807}$ hFc fragment (green) colocalizes with SCs marked by S100β (red) in P10 sciatic nerves. Nuclear counterstain is DAPI (blue). Scale bar = 20 μm in G, H; scale bar = 10 μm in G', H'. (**I**) GPR126$^{N446–807}$ binds Lama2 in vivo. GPR126$^{N446–807}$ and GPR126$^{N31–438}$ proteins were mixed with P3 sciatic nerve lysate and immunoprecipitated with anti-hFc antibodies. Lama2 specifically co-immunoprecipitates with GPR126$^{N446–807}$. Input = 15" exposure, Lama2 = 1' exposure. (**J–K**) Putative ligand binding performed on P10 sciatic nerves of WT and *Lama2*$^{dy3k/dy3k}$ mice. Anti-hFc immunostaining is green and nuclear counterstain is Hoechst 33342 (blue). Magnification of boxed regions in **J–K** (scale bar = 10 μm) is indicated in **J'–K'** (scale bar = 2.7 μm). (**J**) GPR126$^{N446–807}$ binding is robust in WT sciatic nerve, but (**K**) not detected in *Lama2*^{dy3} mutant sciatic nerve.

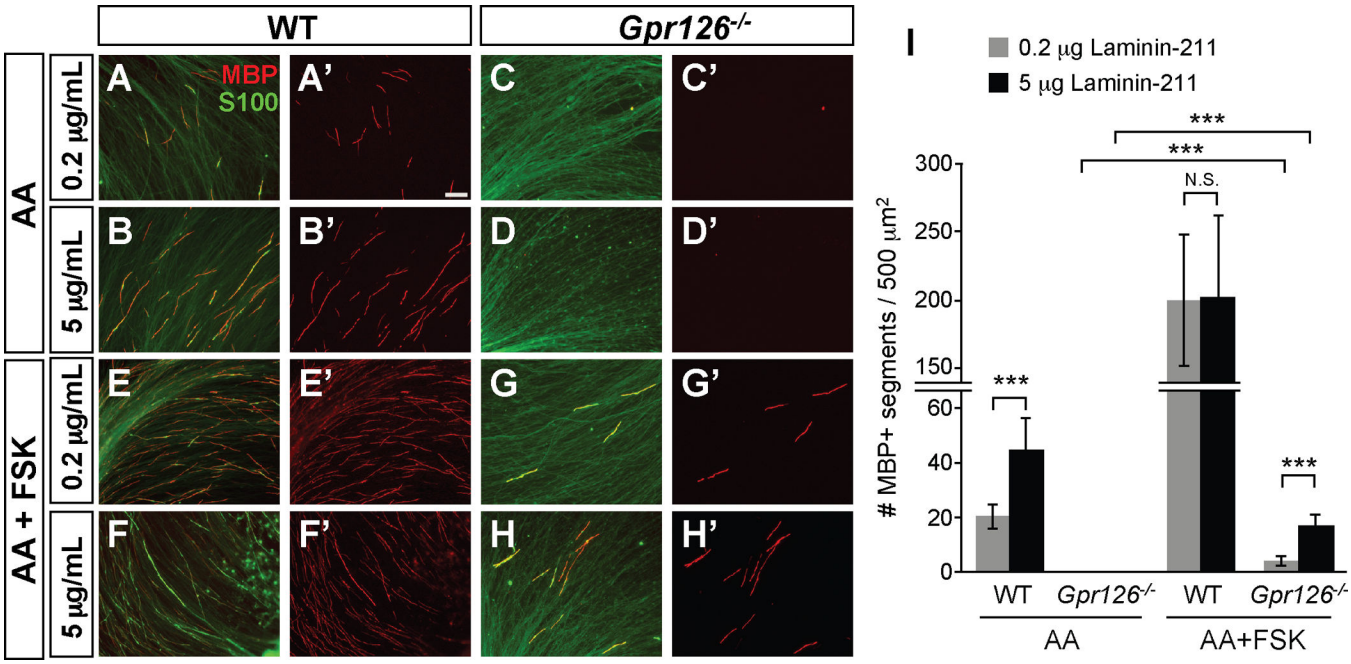

Figure 4. Laminin-211 concentration modulates *in vitro* myelination

(**A–H**) *In vitro* myelination cultures from WT or *Gpr126*$^{-/-}$ DRGs on plates coated with poly-D-lysine + 0.2 or 5 μg/mL Laminin-211. Cultures were immunostained with MBP (red) and S100 (green). Scale bar = 100 μm. (**A–B**) 3 weeks after ascorbic acid (AA) addition in WT, more MBP+ immunostaining is observed on 5 μg/mL Laminin-211 than 0.2 μg/mL 3 weeks after ascorbic acid (AA) addition. (**C–D**) MBP+ immunostaining is not observed in *Gpr126*$^{-/-}$ SCs at any Laminin-211 concentration 3 weeks after AA addition. (**E–F**) Addition of FSK leads to MBP potentiation in WT SCs on both 0.2 and 5 μg/mL Laminin-211 relative to AA alone. (**G–H**) *Gpr126*$^{-/-}$ SCs have low levels of MBP in presence of FSK and show concentration dependence for Laminin-211. (**I**) Quantification of myelination cultures. Bars represent average number of MBP-positive segments per 500 μm^2 + SD. *** p<0.001, Student's t-test, N.S. = no significant difference.

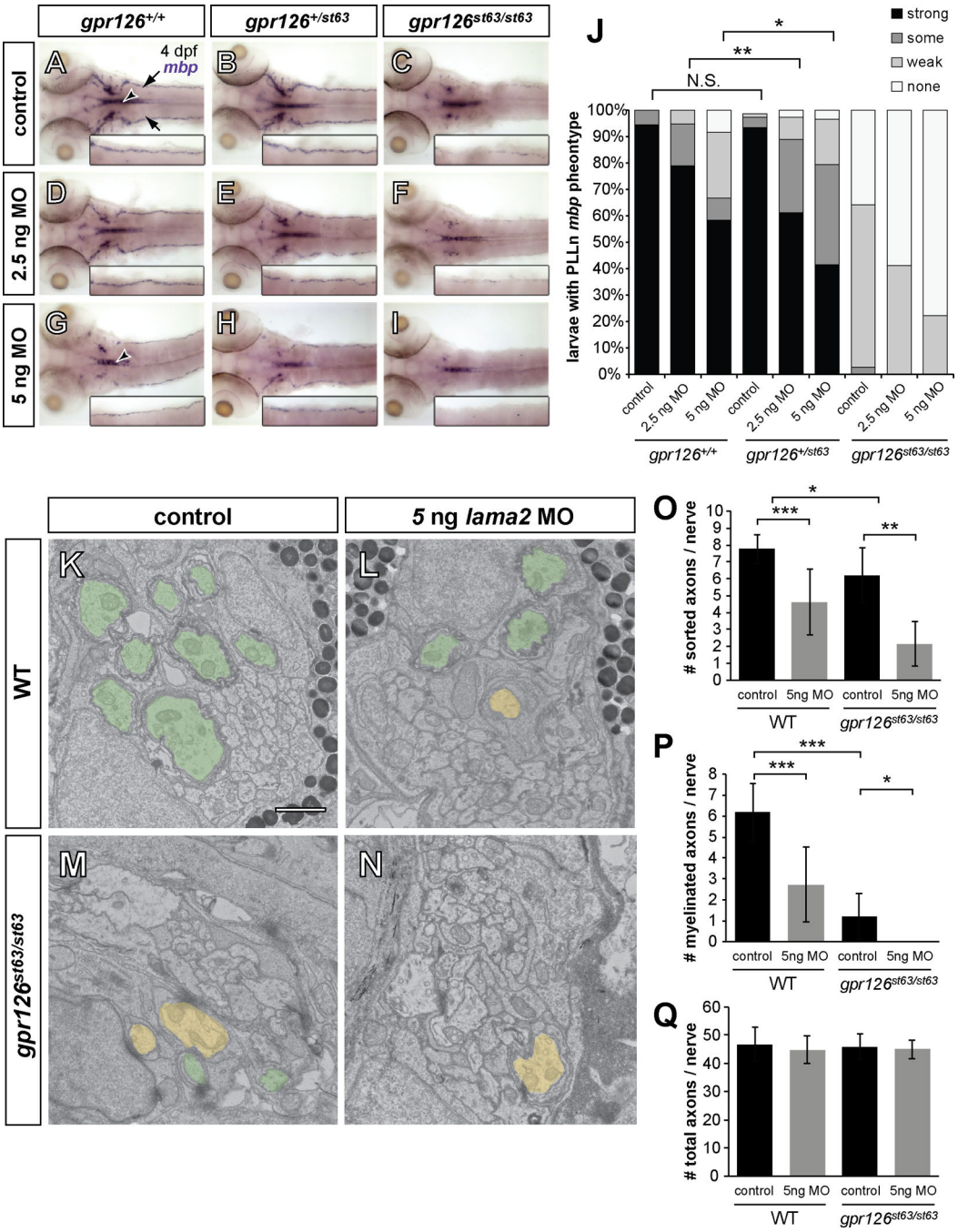

Figure 5. *lama2* knockdown enhances *gpr126* hypomorphic phenotype

(**A–I**) Dorsal views of *mbp* expression by WISH in 4 dpf larvae. Inset panels show magnification of the right PLLn. "Control" = injected with phenol red dye only, "MO" = *lama2* morpholino (MO)-injected. (**A–C**) Control-injected larvae. (**A**) *mbp* expression is strong in the PLLn of a WT (*gpr126*$^{+/+}$) larva. Arrows indicate PLLn, arrowhead indicates CNS. (**B**) *mbp* in heterozygous (*gpr126*$^{+/st63}$) larva is indistinguishable from WT. (**C**) *mbp* is reduced, but not absent, in the PLLn of a homozygous *gpr126*$^{st63/st63}$ hypomorph. (**D–F**) Larvae injected with low dose (2.5 ng) *lama2* MO. (**D**) *mbp* is not disrupted in a *gpr126*$^{+/+}$

larva. (**E**) *mbp* is reduced in the PLLn of a heterozygous *gpr126*$^{+/st63}$ larva relative to control-injected. (**F**) *mbp* is further reduced in a *gpr126*$^{st63/st63}$ larva. (**G–I**) Larvae injected with high dose (5 ng) *lama2* MO. (**G**) *mbp* is disrupted in both the CNS (arrowhead) and PLLn in a *gpr126*$^{+/+}$ larva. (**H**) *mbp* is further reduced in a heterozygous *gpr126*$^{+/st63}$ larva. (**I**) *mbp* is nearly absent in the PLLn of *gpr126*$^{st63/st63}$ larva. (**J**) Quantification of WISH expressed as a percentage of larvae with each *mbp* PLLn phenotype at 4 dpf. Asterisks indicate significant decrease of "strong" expression. * $p<0.05$,** $p<0.01$, Fisher's Exact Test. "Control" = pooled uninjected and phenol red-injected. (**K–N**) 3 dpf zebrafish PLLn TEM. Sorted and myelinated axons are defined and pseudocolored as in Figure 1. Scale bar = 1 μm. (**K**) Myelination proceeds normally in a control-injected *gpr126*$^{+/+}$ sibling, but (**L**) radial sorting and myelination are reduced with 5 ng MO in *gpr126*$^{+/s63}$. (**M**) Myelination is reduced in a *gpr126*$^{st63/st63}$ hypomorph, and is further reduced in (**N**) a *gpr126*$^{st63/st63}$ sibling injected with 5 ng MO. (**O–Q**) Quantification of TEM images. Bars represent means ± SD. * $p<0.05$, ** $p<0.01$, *** $p<0.001$, 1-way ANOVA with Bonferroni's multiple comparisons test. (**O**) Number of sorted axons per PLLn. (**P**) Number of myelinated axons per PLLn. (**Q**) Number of total axons per PLLn.

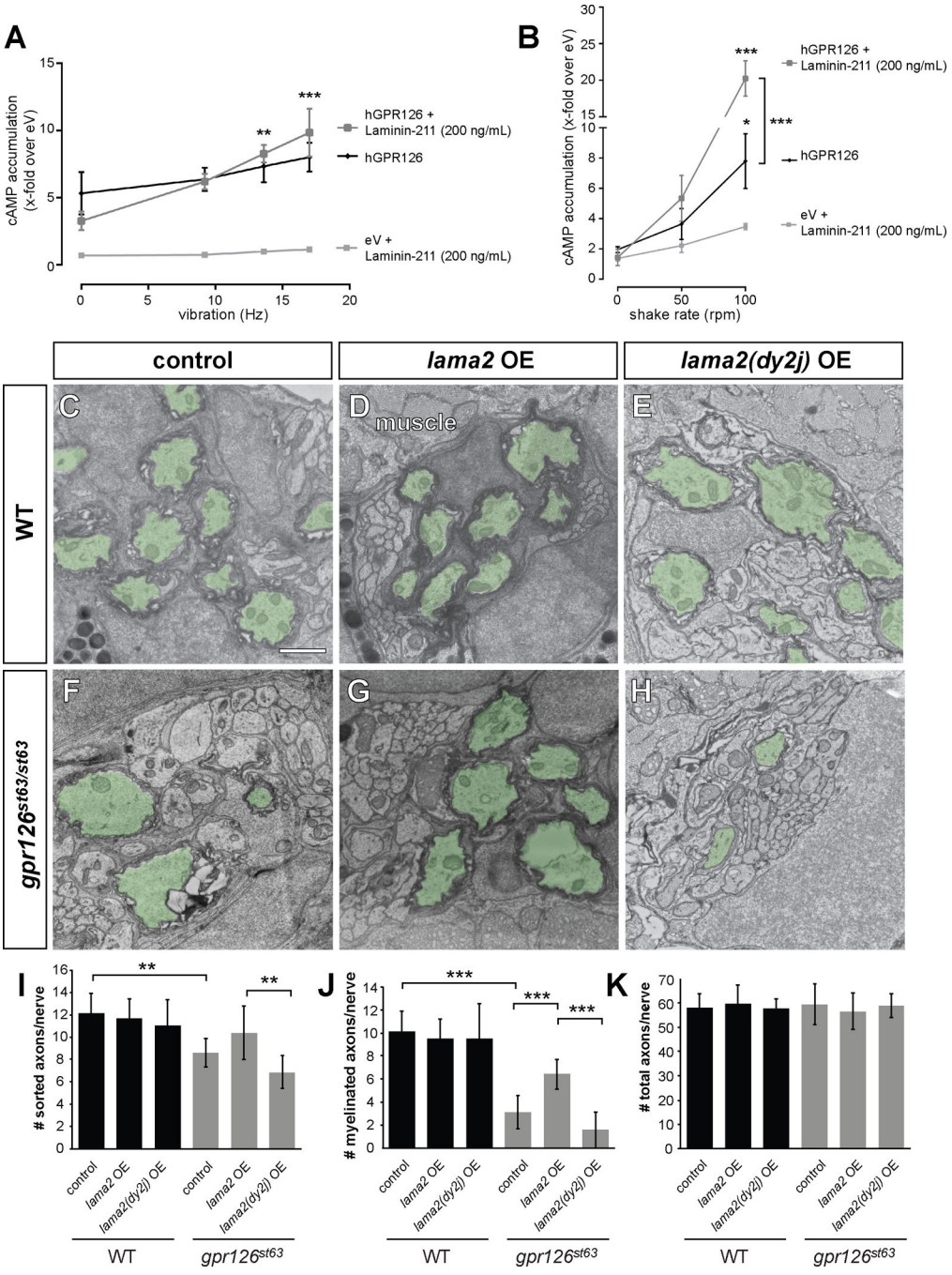

Figure 6. Laminin-211 activates Gpr126 via under dynamic conditions *in vitro* and polymerizing conditions *in vivo*

(**A–B**) COS-7 cells were transiently transfected with empty vector (eV) and hGPR126 plasmid. cAMP accumulation was measured after stimulation with Laminin-211 (200 ng/mL) and indicated force. Data is represented as mean ± SEM of three independent assays each performed in triplicate. * p<0.05; ** p<0.01; *** p<0.001, 2-way ANOVA with Tukey's multiple comparison test (each mechanic-induced response compared to static conditions for all hGPR126 data points, with and without Laminin-211). (**A**) Laminin-211

suppresses GPR126 signaling under stationary conditions (Hz = 0) but causes a frequency-dependent increase of cAMP accumulation with increasing vibration. (**B**) Mechanical stimulation via shaking further enhances Laminin-211-dependent cAMP accumulation with increasing frequency. (**C–H**) TEM of 5 dpf zebrafish PLLn. Myelinated axons are pseudocolored in green. Scale bar = 1 μm. (**C**) Myelination proceeds normally in a control larva, (**D**) in a larva injected with 40 pg WT *lama2* OE construct, and (**E**) in a larva injected with 40 pg mutant *lama2(dy2j)*-OE construct. (**F**) Myelination is reduced in a control-injected *gpr126*$^{st63/st63}$ larva. (**G**) Injection of 40 pg *lama2* OE rescues myelination in a *gpr126*$^{st63/st63}$ larva. (**H**) Injection of 40 pg *lama2*(*dy2j*) OE fails to rescue myelination in a *gpr126*$^{st63/st63}$ larva. (**I–K**) Quantification of TEM images. Bars represent means ± SD. ** $p<0.01$, *** $p<0.001$, 1-way ANOVA with Bonferroni's multiple comparisons test. (**I**) Number of sorted axons per PLLn. (**J**) Number of myelinated axons per PLLn. (**K**) Number of total axons per PLLn.

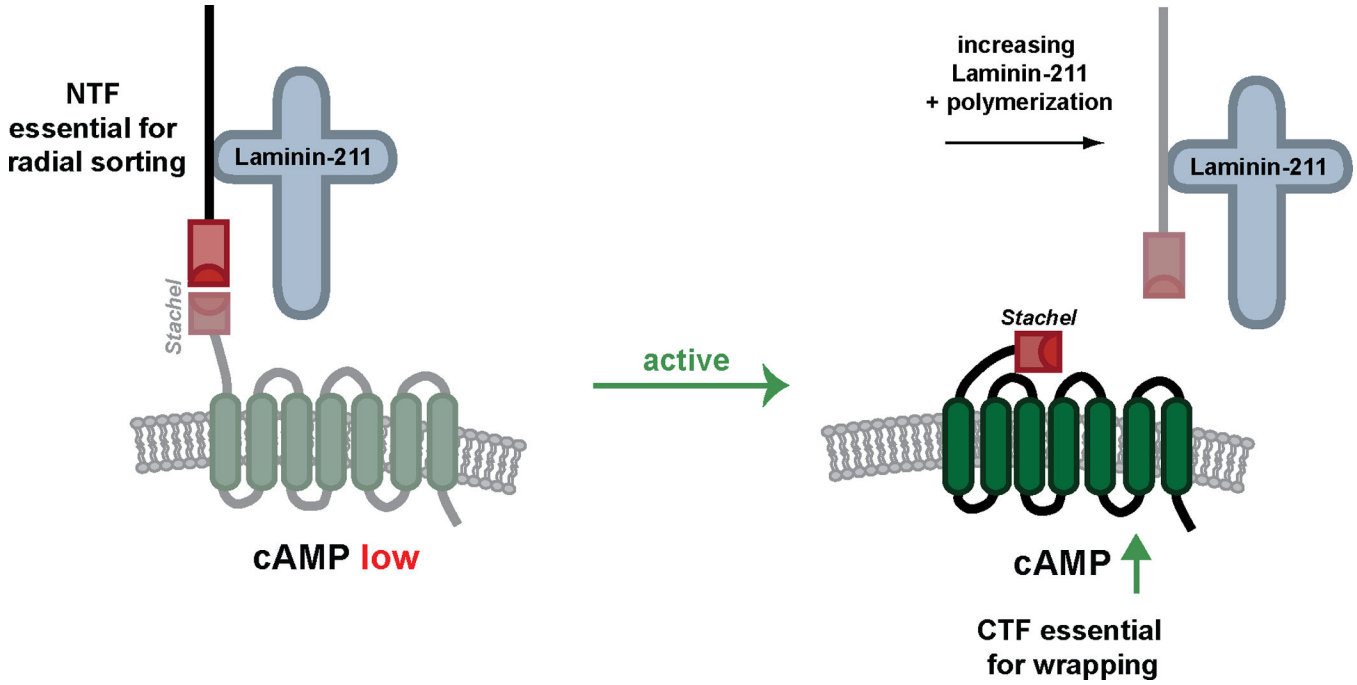

Figure 7. Model for Laminin-211 and GPR126 interactions in SC development

Our data support a model in which Laminin-211 interacts with GPR126-NTF to stabilize the receptor in an inactive state. This prevents cAMP accumulation through suppression of basal GPR126 G_s signaling and allows the SC to remain in an immature state for radial sorting. Independent of Gpr126-CTF, Gpr126-NTF is required for radial sorting. Following BL maturation and Laminin-211 polymerization, Laminin-211 facilitates an active G_s signaling conformation of GPR126-CTF. This may be accomplished by removal of GPR126-NTF via mechanical forces induced during Laminin-211 polymerization. G_s signaling promotes cAMP accumulation, downstream signaling, and terminal differentiation of the SC.